Combined effects of optical and acoustic birefringence on acousto-optic mode coupling in photonic crystal fiber

Sun Do Lim[1]*, Hyun Chul Park[1], In Kag Hwang[2], and Byoung Yoon Kim[1]

[1]*Department of Physics, Korea Advanced Institute of Science and Technology, 373-1 Guseong-dong, Yuseong-gu, Daejeon 305-701, Korea*

[2]*Department of Physics, Chonnam National University, 300 Yongbong-dong, Buk-gu, Gwangju, 500-757, Korea*

* *dukelim@kaist.ac.kr*

http://fiber.kaist.ac.kr

Abstract: We investigate in detail the origin of multiple resonance peaks experimentally observed in an all-fiber acousto-optic tunable filter built with a photonic crystal fiber having slightly deformed air-hole structure and non-circular outer cladding. A model for the acousto-optic mode coupling in the PCF is formulated taking into account both the acoustic and the optical birefringence. All experimental results are in good agreement with numerical calculations.

OCIS codes: (060.2310) Fiber optics; (230.1040) Acousto-optical devices; (060.2270) Gratings; (060.5295) photonic crystal fiber.

References and links

1. H. S. Kim, S. H. Yun, I. K. Hwang, and B. Y. Kim, "All-fiber acousto-optic tunable notch filter with electronically controllable spectral profile," Opt. Lett. **22**, 1476-1478 (1997).
2. K. J. Lee, D. I. Yeom, and B. Y. Kim, "Narrowband, polarization insensitive all-fiber acousto-optic tunable bandpass filter," Opt. Express **15**, 2987-2992 (2007).
3. B. Y. Kim, J. N. Blake, H. E. Engan, and H. J. Shaw, "All-fiber acousto-optic frequency shifter," Opt. Lett. **11**, 389-391 (1986).
4. T. Jin, Q. Li, J. Zhao, K. Cheng, and X. Liu, "Ultra-Broad-Band AOTF Based on Cladding Etched Single-Mode Fiber," IEEE Photon. Technol. Lett. **14**, 1133–1135 (2002).
5. D. I. Yeom, H. S. Kim, M. S. Kang, H. S. Park, and B. Y. Kim, "Narrow-Bandwidth All-Fiber Acoustooptic Tunable Filter With Low Polarization-Sensitivity," IEEE Photon. Technol. Lett. **17**, 2646–2648 (2005).
6. J. C. Knight, T. A. Birks, P. St. J. Russell, and D. M. Atkin, "All-silica single-mode optical fiber with photonic crystal cladding," Opt. Lett. **21**, 1547-1549 (1996).
7. A. Ortigosa-Blanch, J. C. Knight, W. J. Wadsworth, J. Arriaga, B. J. Mangan, T. A. Birks, and P. St. J. Russell, "Highly birefringent photonic crystal fibers," Opt. Lett. **25**, 1325-1327 (2000).
8. W. H. Reeves, J. C. Knight, P. J. Roberts, and P. St. J. Russell, "Demonstration of ultra-flattened dispersion in photonic crystal fibers," Opt. Express **10**, 609-613 (2002).
9. A. Diez, A. Birks, W. H. Reeves, B. J. Mangan, and P. St. J. Russell, "Excitation of cladding modes in photonic crystal fibers by flexural acoustic waves," Opt. Lett. **25**, 1499-1501 (2000).
10. K. S. Hong, H. C. Park, I. K. Hwang, W. Jin, J. Ju, D. I. Yeom, and B. Y. Kim "1000 nm tunable acousto-optic filter based on photonic crystal fiber," Appl. Phys. Lett. **92**, 031110 (2008).
11. D-I. Yeom, P. Steinvurzel, B. J. Eggleton, S. D. Lim, and B. Y. Kim, "Tunable acoustic gratings in solid-core photonic bandgap fiber," Opt. Express **15**, 3513-3518 (2007).
12. M. W. Haakestad and H. E. Engan, "Acoustooptic properties of a weakly multimode solid core photonic crystal fiber," J. Lightwave Technol. **24**, 838-845 (2006).
13. M. W. Haakestad and H. E. Engan, "Acoustooptic characterization of a birefringent two-mode photonic crystal fiber," Opt. Express **14**, 7319-7328 (2006).
14. S. G. Johnson and J. D. Joannopoulos, "Block-iterative frequency-domain methods for Maxwell's equations in a planewave basis," Opt. Express **8**, 173-190 (2001).
15. Y-J. Lee, D-S. Song, S-H. Kim, J. Huh, and Y-H. Lee, "Modal characteristics of photonic crystal fibers," J. Opt. Soc. Korea **7**, 47-52 (2003).
16. R. Guobin, W. Zhi, L. Shuqin, and J. Shuisheng, "Mode classification and degeneracy in photonic crystal fibers," Opt. Express **11**, 1310-1321 (2003).
17. N. A. Mortensen, M. D. Nielsen, J. R. Folkenberg, K. P. Hansen, and J. Lægsgaad, "Small-core photonic crystal fibers with weakly disordered air-hole claddings," J. Opt. A **6**, 221-223 (2004).

#92144 - $15.00 USD Received 28 Jan 2008; revised 3 Apr 2008; accepted 6 Apr 2008; published 16 Apr 2008

18. H. E. Engan, B. Y. Kim, J. N. Blake, and H. J. Shaw, "Propagation and optical interaction of guided acoustic waves in two-mode optical fibers," J. Lightwave Technol. **6**, 428–436 (1988).
19. P. R. McIsaac, "Symmetry-induced modal characteristics of uniform waveguides-I. Summary of results," IEEE Trans. Microwave Theory Tech. MTT-23, 421-429 (1975).
20. B. Langli and K. Bløtekjær, "Effect of acoustic birefringence on acoustooptic interaction in birefrengent two-mode optical fibers," J. Lightwave Technol. **21**, 528-535 (2003).
21. M. V. Andres, M. J. Tudor, and K. W. H. Foulds, "Analysis of an interferometric optical fibre detection technique applied to silicon vibrating sensors," Electron. Lett. **23**, 774-775 (1987).
22. Amnon Yariv, "Coupled mode theory for guided-wave optics," IEEE J. Quantum Electron. **9**, 919-933 (1973).

1. Introduction

Acousto-optic (AO) mode coupling in optical fibers has been used in a number of optical devices such as notch filters [1], band pass filters [2], and frequency shifters [3]. The device characteristics are largely determined by the optical properties of the fibers used [4, 5]. The introduction of photonic crystal fiber (PCF) [6] opened up possibilities of fiber devices with novel features because its optical properties can be easily tailored by changing air-hole geometry in the PCFs [7, 8]. In recent years, many reports have been made for PCF-based AO devices with interesting filter properties using flexural acoustic wave traveling along the fiber. [9-11]. One of the undesirable features observed in these AO filters was that the spectral shape of the filters was distorted having multiple resonance peaks [11, 12]. Since the distortion of the filter spectrum will severely limit the practical applications of the filters, it is important to determine the origin of the phenomena and find ways to control it. It has been speculated that the origin of such distorted filter spectra is the refractive index splitting between nearly degenerate higher-order modes and/or the axial non-uniformities of the fiber [12, 13]. However, no systematic analysis has been reported to quantitatively explain the observed filter behavior, to the best of our knowledge.

In this paper, we successfully explain the origin of the multiple resonance peaks experimentally observed in an all-fiber acousto-optic tunable filter (AOTF) as a result of an interplay between acoustic and optical birefringence in the PCF. Both acoustic and optical birefringence come from the structural imperfections of the fiber and the experimental results are in good agreement with numerical calculations and simulations.

2. Optical and acoustic birefringence in an imperfectly structured PCF

The PCF used in the experiment is a commercially available PCF, which has inversion and six-fold rotation symmetry of the air-hole lattice surrounding a silica core as shown in Fig. 1.

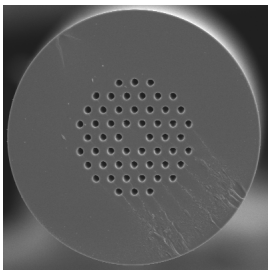

Fig. 1. SEM images of cleaved PCF end face

Scanning electronic microscope images (SEMs) were used to determine geometric parameters of the PCF. Average values of the air-hole diameter (d) and the pitch (center-to-center distance between the holes, Λ) are 3.8 μm, and 8.2 μm, respectively. Numerical calculation using plane wave expansion method [14, 15] based on these parameters reveals that the PCF supports only six guided modes in the silica core over the optical wavelength ranging from 600 to 1300 nm, where our experiment was carried out. For a perfectly structured PCF with

#92144 - $15.00 USD Received 28 Jan 2008; revised 3 Apr 2008; accepted 6 Apr 2008; published 16 Apr 2008

C_{6v} symmetry, the first higher-order modes resemble the TM_{01}, TE_{01}, and HE_{21} modes of a standard fiber [16]. However, any slight disorder in the inner air-hole lattice can make them split into the LP_{11} modes resembling those in elliptical-core two-mode fibers [17]. We therefore precisely measured the diameter and the pitch of the six inner air holes, and their variations were found to be up to 2% and 3%, respectively. Taking these results into account, the guided core modes in the PCF were recalculated. They are summarized in Fig. 2, which depicts the electric field and intensity distributions of the LP_{01} and the LP_{11} modes at 1280 nm.

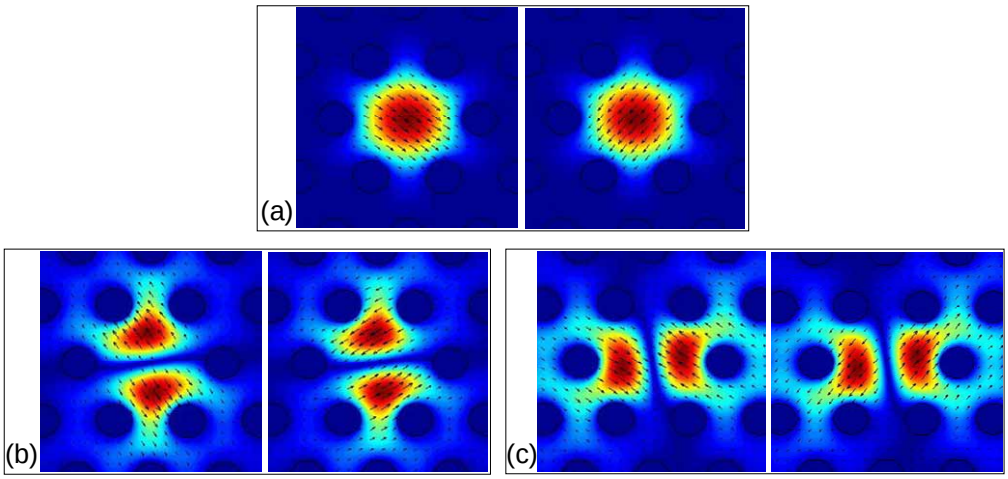

Fig. 2. Calculated electric field distributions of (a) the LP_{01} modes, (b) the even LP_{11} modes, and (c) the odd LP_{11} modes.

Figure 2(a) shows that the LP_{01} mode has two eigen-polarization states as it is in the circular step-index fiber. On the other hand, the LP_{11} modes are split into two groups that are called the even and the odd LP_{11} modes with a set of symmetry axes (optical eigen axes) as shown in Figs. 2(b) and 2(c). Here, the even and the odd LP_{11} modes are defined as those with the higher and the lower mode effective refractive indices, respectively. Each of the even and the odd LP_{11} modes has also two eigen-polarization states. It is obvious that the fundamental mode has a smaller fraction of the near field in the air holes than the higher-order modes. Consequently, the LP_{01} mode is less sensitive to the disorders of the air-hole lattice than the LP_{11} modes. This explains why the LP_{01} mode has the same refractive index between the eigen-polarization states within calculation error of $1x10^{-7}$, whereas the second-order modes have the refractive index difference of $3x10^{-5}$ between the even and the odd LP_{11} modes, which is much greater than that between the two eigen-polarization states in each of the LP_{11} mode groups at about $1x10^{-6}$.

Optical fibers including PCFs are also good acoustic waveguides with low loss for the lowest-order flexural acoustic wave which is used in acousto-optic devices [18]. According to the previous studies, two orthogonal vibration modes of the lowest-order flexural acoustic wave propagating along a PCF with hexagonal air-hole symmetry have the same phase velocity, and their acoustic properties are the same to those of circular rods [19, 12]. However, in real situation, optical fibers often have elliptical shape in their outer cladding, which provides the acoustic phase velocity difference between the ellipse axes (acoustic eigen axes) [20]. In contrast to the case of the optical birefringence, the irregularity of the air holes in the PCF has little influence on the acoustic birefringence compared to the cladding ellipticity [12]. The average diameter of the PCF's outer cladding was 125 μm. In order to determine the ellipticity of the outer cladding, we experimentally measured the phase velocity of flexural acoustic waves at different vibration directions using an interferometric fiber probe [21]. The

#92144 - $15.00 USD Received 28 Jan 2008; revised 3 Apr 2008; accepted 6 Apr 2008; published 16 Apr 2008

result shows non-negligible acoustic phase velocity difference of 0.19 ± 0.02% at the applied acoustic frequency of 3.3 MHz. The ellipticity is obtained from the result to be about 0.4 ± 0.05%, which was verified by direct measurement from SEM images of cleaved end face of the PCF. Here, the ellipticity is defined as the ratio of the diameter difference between the major and the minor axes of the cladding ellipse to the average cladding diameter.

Note that the optical properties of the guided modes are determined by the air-hole structure around the core, and the acoustic properties are determined primarily by the outer cladding geometry. In the next section, we will discuss about the acousto-optic mode coupling in the PCF based on the angular relation between the acoustic and the optical eigen axes.

3. Acousto-optic mode coupling in the PCF

In the previous section, the acoustic and the optical eigen axes were defined. Unless these two sets of axes coincide with each other, the coupling of the LP_{01} mode to the even and the odd LP_{11} modes will be simultaneously introduced by a flexural acoustic wave, which results in multiple peaks in the output spectrum. Therefore, possible angular misalignment between the acoustic and optical axes should be verified. Figure 3(a) shows the major and the minor axes of the outer cladding ellipse along with the intensity lobe orientation of the even and the odd LP_{11} modes. The lobe orientation could easily be determined experimentally because their resonance peaks occur at different acoustic frequencies for a given optical wavelength. The two near-field optical images were taken at 633 nm with a 25× microscopic lens and a CCD camera. The misalignment between the two directions representing the acoustic and optical axes is clearly seen, and the angle α is about $\pi/6$.

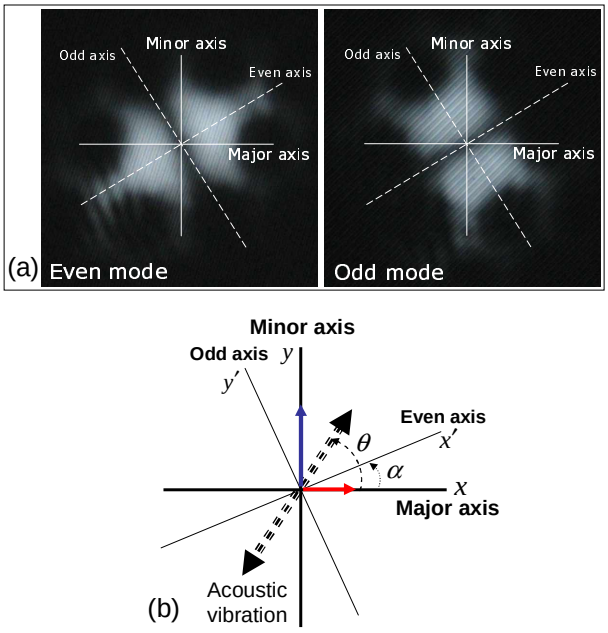

Fig. 3. (a). Microscopic images of near fields of the even LP_{11} mode and the odd LP_{11} modes at 633 nm after alignment of the major and minor axes of the cladding ellipse along the laboratory frame, respectively. (b) Diagram of the angular misalignment between the acoustic and optical axes for modeling of AO mode coupling in the fiber.

Here, the optical even and odd axes are defined as the intensity lobe direction of the even and the odd LP_{11} modes, respectively. When a flexural acoustic wave is launched at $z = 0$ with its vibration angle at θ as shown in Fig. 3(b), the coupling strength $\kappa(z)$ between the LP_{01} mode and two LP_{11} mode groups can be formulated by a simple trigonometric decomposition as follow.

#92144 - $15.00 USD Received 28 Jan 2008; revised 3 Apr 2008; accepted 6 Apr 2008; published 16 Apr 2008

$$\kappa(z)=\begin{pmatrix}\kappa_{x'(even)}(z)\\ \kappa_{y'(odd)}(z)\end{pmatrix}=\kappa_0\begin{pmatrix}\sin\theta\sin\alpha e^{i\frac{2\pi}{\Lambda_s}z}+\cos\theta\cos\alpha e^{i\frac{2\pi}{\Lambda_l}z}\\ \sin\theta\cos\alpha e^{i\frac{2\pi}{\Lambda_s}z}-\cos\theta\sin\alpha e^{i\frac{2\pi}{\Lambda_l}z}\end{pmatrix} \quad (1)$$

The $\kappa(z)$ consists of two coupling strengths of $\kappa_{x'}(z)$ and $\kappa_{y'}(z)$ that represent the coupling strengths between the LP_{01} mode and the even and the odd LP_{11} modes, respectively, and κ_0 is the coupling strength when $\theta = 0$ and $\alpha = 0$. z is the propagation length. The Λ_l and the Λ_s are the acoustic wavelengths along the major and the minor axes of the cladding ellipse, respectively.

In cases of $\theta = 0$ or $\theta = \pi$, each component has only one phase term of Λ_l as follow.

$$\kappa(z)=\begin{pmatrix}\kappa_{x'(even)}(z)\\ \kappa_{y'(odd)}(z)\end{pmatrix}=\kappa_0\begin{pmatrix}\pm\cos\alpha e^{i\frac{2\pi}{\Lambda_l}z}\\ \mp\sin\alpha e^{i\frac{2\pi}{\Lambda_l}z}\end{pmatrix} \quad (2)$$

where upper and lower signs of each coupling strength are for cases of $\theta = 0$ or $\theta = \pi$, respectively. Phase matching conditions for the upper and the lower coupling strengths are $2\pi/L_B^{LP01\text{-}LP11even} = 2\pi/\Lambda_l$ and $2\pi/L_B^{LP01\text{-}LP11odd} = 2\pi/\Lambda_l$, respectively. The L_B means optical beat length between two modes. In cases of $\theta = \pi/2$ or $\theta = 3\pi/2$, each coupling strength has also only one phase term of Λ_s, which is

$$\kappa(z)=\begin{pmatrix}\kappa_{x'(even)}(z)\\ \kappa_{y'(odd)}(z)\end{pmatrix}=\kappa_0\begin{pmatrix}\pm\sin\alpha e^{i\frac{2\pi}{\Lambda_s}z}\\ \pm\cos\alpha e^{i\frac{2\pi}{\Lambda_s}z}\end{pmatrix} \quad (3)$$

where the upper and the lower signs are for cases of $\theta = \pi/2$ or $\theta = 3\pi/2$, respectively. Phase matching conditions for the upper and the lower coupling strengths are $2\pi/L_B^{LP01\text{-}LP11even} = 2\pi/\Lambda_s$ and $2\pi/L_B^{LP01\text{-}LP11odd} = 2\pi/\Lambda_s$, respectively.

On the other hand, in case of $\theta \neq n\pi/2$ (n is the integer number), each coupling strength consists of a linear combination of two components having phase terms of Λ_l and Λ_s with different portion of amplitude as a function of θ and α in the Eq. (1). This represents that two projected components of traveling flexural acoustic waves along acoustic major and minor axes are superposed on the optical axes, which gives rise to an acoustic amplitude beating along the optical axes. In order to describe the effect of the acoustic amplitude beating on the AO coupling, we employ the simplest form of coupling strengths by assuming $\alpha = \pi/4$ and $\theta = \pi/4$. Then, the corresponding expression is given by

$$\kappa(z)=\begin{pmatrix}\kappa_{x'(even)}(z)\\ \kappa_{y'(odd)}(z)\end{pmatrix}=\frac{\kappa_0}{2}\begin{pmatrix}e^{i\frac{2\pi}{\Lambda_s}z}+e^{i\frac{2\pi}{\Lambda_l}z}\\ e^{i\frac{2\pi}{\Lambda_s}z}-e^{i\frac{2\pi}{\Lambda_l}z}\end{pmatrix}=\kappa_0 e^{ik_{ave}z}\begin{pmatrix}\cos(k_{\mathrm{mod}}z)\\ i\sin(k_{\mathrm{mod}}z)\end{pmatrix} \quad (4)$$

where, $k_{ave} = \pi/\Lambda_s + \pi/\Lambda_l$ and $k_{mod} = \pi/\Lambda_s - \pi/\Lambda_l$. The coupling strengths of the even LP_{11} mode (upper part) and of the odd LP_{11} mode (lower part) in Eq. (4) contain the cosine and the sine functions, respectively. The two modulation functions results in a significant difference in the output spectrum, especially when the value of $k_{mod} \cdot L_c$ is about π. L_c denotes the total AO interaction length. In such case, the sign of coupling strength in the upper part of the Eq. (4) is minus when the relative phase difference ($k_{mod}z$) between two acoustic waves is over the range from $\pi/2$ to π. It means that the coupled light to the LP_{11} mode that satisfies the phase

#92144 - $15.00 USD Received 28 Jan 2008; revised 3 Apr 2008; accepted 6 Apr 2008; published 16 Apr 2008

matching condition is coupled back to the LP_{01} mode over the range of $\pi/2 \leq k_{mod}z \leq \pi$. Therefore, the net AO coupling is zero at the resonant wavelength, which leads a notch to be split in transmission as shown in Fig. 4(a). On the other hand, the sign of coupling strength in the lower part of the Eq. (4) is still plus through the region of $\pi/2 \leq k_{mod}z \leq \pi$, so that the light in the LP_{01} mode is maximally coupled to the LP_{11} mode at the resonant wavelength as shown in Fig. 4(b).

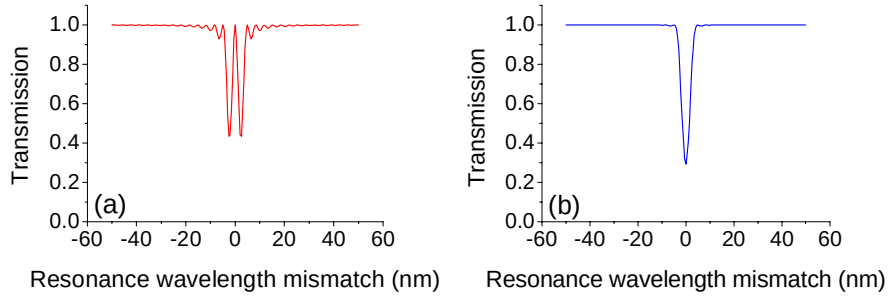

Fig. 4. Calculated transmission spectra when an acoustic grating suffers from (a) cosine amplitude modulation and (b) sine amplitude modulation, respectively.

4. Experiment and analysis

The AO mode coupling as a function of circumferential angle of initial acoustic vibration on the fiber cross-section was performed by employing AOTF as shown in Fig. 5.

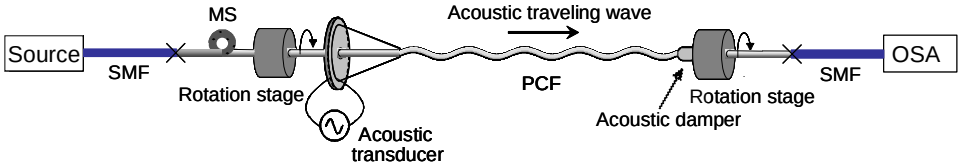

Fig. 5. A schematic of the AOTF (SMF: single mode fiber, MS: mode stripper, OSA: optical spectrum analyzer).

The basic configuration of the device is similar to that described in Ref. 1. The lowest-order flexural acoustic wave generated by acoustic transducer propagates along a 25-cm long bare section of untwisted and straight fiber before it is absorbed by acoustic damper at the end of the interaction region. The periodic perturbation introduced by acoustic wave produces coupling between two optical modes when phase matching condition is satisfied in that the acoustic wavelength is the same as the beat length between two modes. The vibration direction of the flexural acoustic wave at the input can be adjusted by rotation stages holding both ends of the striped section of the fiber.

Figure 6 shows the filtering spectra of the AOTF with a 25-cm-long interaction length at applied acoustic frequency of 3.3 MHz for a broadband unpolarized input light from a LED with center wavelength of 1280 nm in two cases of $\theta = 0$ (acoustic wave is initially excited along the major axis) and $\theta = \pi/2$ (acoustic wave is initially excited along the minor axis).

#92144 - $15.00 USD Received 28 Jan 2008; revised 3 Apr 2008; accepted 6 Apr 2008; published 16 Apr 2008

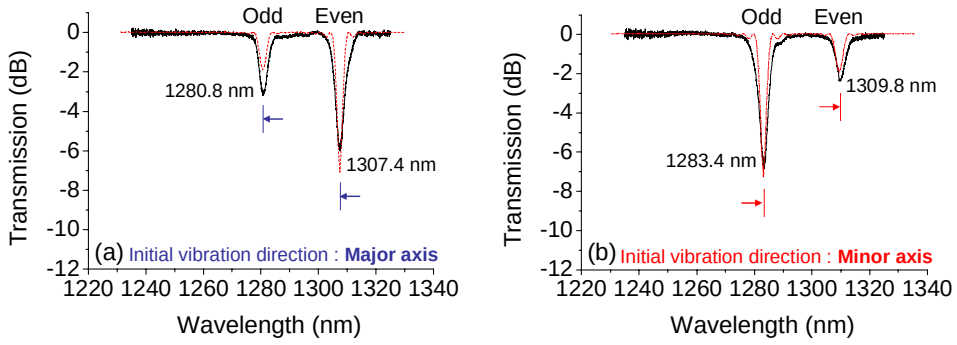

Fig. 6. Measured transmission spectra when an acoustic vibration direction is parallel to (a) major axis, and (b) minor axis. (Doted line: calculation).

The corresponding coupling coefficients are given by

$$\kappa_{\theta=0}(z)=\begin{pmatrix}\kappa_{x'(even)}(z)\\ \kappa_{y'(odd)}(z)\end{pmatrix}=\kappa_0\begin{pmatrix}\frac{\sqrt{3}}{2}e^{i\frac{2\pi}{\Lambda_l}z}\\ -\frac{1}{2}e^{i\frac{2\pi}{\Lambda_l}z}\end{pmatrix} \qquad \kappa_{\theta=\frac{\pi}{2}}(z)=\begin{pmatrix}\kappa_{x'(even)}(z)\\ \kappa_{y'(odd)}(z)\end{pmatrix}=\kappa_0\begin{pmatrix}\frac{1}{2}e^{i\frac{2\pi}{\Lambda_s}z}\\ \frac{\sqrt{3}}{2}e^{i\frac{2\pi}{\Lambda_s}z}\end{pmatrix} \tag{5}$$

For the theoretical prediction, coupled mode equations [22] are calculated with the coupling strengths in Eq. (1) by using the fourth-order runge-kutta method. Straight and dashed lines in the figure denote experimental and calculation results, respectively, and they are in good agreement. As expected from the discussions for the Eqs. (2) and (3), each spectrum has two resonant notches due to two phase matching conditions of the LP_{01} - the even LP_{11} mode and the LP_{01} - the odd LP_{11} mode. The resonant wavelengths satisfying the phase matching conditions of $2\pi/L_B^{LP01\text{-}LP11odd} = 2\pi/\Lambda_l$, $2\pi/L_B^{LP01\text{-}LP11even} = 2\pi/\Lambda_l$, $2\pi/L_B^{LP01\text{-}LP11odd} = 2\pi/\Lambda_s$, and $2\pi/L_B^{LP01\text{-}LP11even} = 2\pi/\Lambda_s$ are 1280.8, 1307.4, 1283.4, and 1309.8 nm, respectively. The position of two notches in Fig. 6(b) are up-shifted compared to those in Fig. 6(a) by about 2.5 nm, that compares well with 2.7 nm obtained from the calculation considering the acoustic wavelength difference of about 1 μm and the optical beat length curves. The spacing between two notches is about 26.5 nm, which is also in good agreement with theoretical calculation of 26.1 nm considering the index difference of 3×10^{-5} between the even and the odd LP_{11} modes.

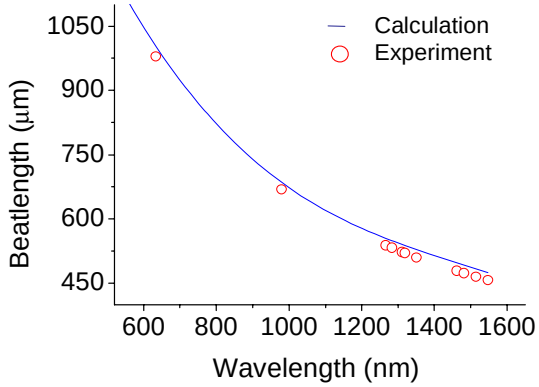

Fig. 7. Measured and calculated optical beatlength between the LP_{01} and the even LP_{11} modes as a function of optical wavelength.

#92144 - $15.00 USD Received 28 Jan 2008; revised 3 Apr 2008; accepted 6 Apr 2008; published 16 Apr 2008

Optical polarization mode splitting in each case was less than 0.2 nm in transmission spectra, which agrees well with the calculated value of less than 0.5 nm for the index difference of about 1×10^{-6} between eigen-polarization states of both the LP_{11} modes. Notch depth difference between two peaks in each figure is due to the coupling strength difference as shown in Eq. (5). The optical beatlength between the LP_{01} and the even LP_{11} modes with respect to the optical wavelength is obtained both experimentally and theoretically, which are plotted as shown in Fig. 7. The optical beatlength between the LP_{01} and the odd LP_{11} modes with respect to the optical wavelength is similar to that in Fig. 7.

More complex notch peaks appear when the acoustic vibration direction does not coincide with the acoustic axes of the PCF at the input, because the effect of acoustic birefringence emerges in the filtering spectra. Firstly, we increased the angle from $\theta = 0$ to $\pi/2$ by rotating the PCF and observed the output spectra at three different angles of $\theta = \pi/6$, $\pi/4$, and $\pi/3$. The corresponding coupling strengths deduced from the Eq. (1) are as follows.

$$\kappa_{\theta=\frac{\pi}{6}} = \kappa_0 \begin{pmatrix} \frac{1}{4}e^{i\frac{2\pi}{\Lambda_s}z} + \frac{3}{4}e^{i\frac{2\pi}{\Lambda_l}z} \\ \frac{\sqrt{3}}{4}e^{i\frac{2\pi}{\Lambda_s}z} - \frac{\sqrt{3}}{4}e^{i\frac{2\pi}{\Lambda_l}z} \end{pmatrix} \quad \kappa_{\theta=\frac{\pi}{4}} = \kappa_0 \begin{pmatrix} \frac{\sqrt{2}}{4}e^{i\frac{2\pi}{\Lambda_s}z} + \frac{\sqrt{6}}{4}e^{i\frac{2\pi}{\Lambda_l}z} \\ \frac{\sqrt{6}}{4}e^{i\frac{2\pi}{\Lambda_s}z} - \frac{\sqrt{2}}{4}e^{i\frac{2\pi}{\Lambda_l}z} \end{pmatrix} \quad \kappa_{\theta=\frac{\pi}{3}} = \kappa_0 \begin{pmatrix} \frac{\sqrt{3}}{4}e^{i\frac{2\pi}{\Lambda_s}z} + \frac{\sqrt{3}}{4}e^{i\frac{2\pi}{\Lambda_l}z} \\ \frac{3}{4}e^{i\frac{2\pi}{\Lambda_s}z} - \frac{1}{4}e^{i\frac{2\pi}{\Lambda_l}z} \end{pmatrix} \quad (6)$$

The summation and subtraction of the two exponential terms of Λ_s and Λ_l in the coupling strengths of the even LP_{11} modes (upper parts) and of the odd LP_{11} modes (lower parts) in Eq. 6 represent the cosinusoidal and sinusoidal beating that affect the even and the odd LP_{11} mode coupling, respectively. In our experiment, the relative phase difference ($k_{mod}z$) is ranging from 0 to $9\pi/10$. Therefore, the notch splitting phenomenon is reasonably expected for the couplings to the even LP_{11} modes (upper parts), whereas it is not expected for the couplings to the odd LP_{11} mode (lower parts). They are summarized in Fig. 8 exhibiting three filtering spectra for cases of $\theta = \pi/6$, $\pi/4$, and $\pi/3$, respectively.

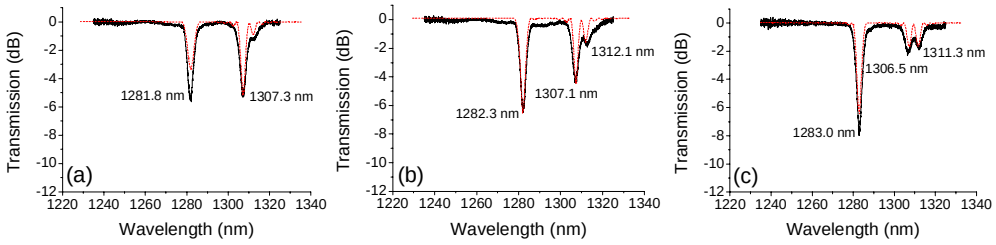

Fig. 8. Measured transmission spectra when initial acoustic vibration angles θ are (a) $\pi/6$, (b) $\pi/4$, and (c) $\pi/3$. (Doted line: calculation).

The asymmetric notch shapes for the even LP_{11} mode coupling as shown in Figs. 8(a) and 8(b) are attributed to the different magnitudes of two exponential terms. The interesting feature for the odd LP_{11} mode couplings is that the maximum notch moves from 1281.8 ($\theta = \pi/6$) to 1283.0 nm ($\theta = \pi/3$) as the angle θ increases. It is because the fraction of the coupling strength having phase term of Λ_s becomes larger. Therefore, as the angle θ increases from 0 to $\pi/2$, the main peak moves from the resonant wavelength satisfying the phase matching conditions of $2\pi/L_B^{LP01\text{-}LP11odd} = 2\pi/\Lambda_l$ to that of $2\pi/L_B^{LP01\text{-}LP11odd} = 2\pi/\Lambda_s$, which are 1280.8 and 1283.4 nm, respectively. Nextly, we also performed the same experiments over the range from $\theta = \pi/2$ to π and the output spectra were obtained at three different angles of $2\pi/3$, $3\pi/4$, and $5\pi/6$. Figure 9 shows three filtering spectra for cases of $\theta = 2\pi/3$, $3\pi/4$, and $5\pi/6$, respectively and the corresponding coupling coefficients are given by

#92144 - $15.00 USD Received 28 Jan 2008; revised 3 Apr 2008; accepted 6 Apr 2008; published 16 Apr 2008

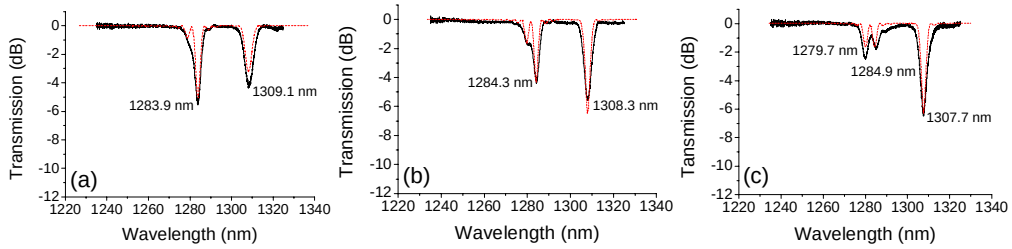

Fig. 9. Measured transmission spectra when initial acoustic vibration angles θ are (a) 2π/3, (b) 3π/4, and (c) 5π/6. (Doted line: calculation).

$$\kappa_{\theta=\frac{2\pi}{3}} = \kappa_0 \begin{pmatrix} \frac{\sqrt{3}}{4} e^{i\frac{2\pi}{\Lambda_s}z} - \frac{\sqrt{3}}{4} e^{i\frac{2\pi}{\Lambda_l}z} \\ \frac{3}{4} e^{i\frac{2\pi}{\Lambda_s}z} + \frac{1}{4} e^{i\frac{2\pi}{\Lambda_l}z} \end{pmatrix} \quad \kappa_{\theta=\frac{3\pi}{4}} = \kappa_0 \begin{pmatrix} \frac{\sqrt{2}}{4} e^{i\frac{2\pi}{\Lambda_s}z} - \frac{\sqrt{6}}{4} e^{i\frac{2\pi}{\Lambda_l}z} \\ \frac{\sqrt{6}}{4} e^{i\frac{2\pi}{\Lambda_s}z} + \frac{\sqrt{2}}{4} e^{i\frac{2\pi}{\Lambda_l}z} \end{pmatrix} \quad \kappa_{\theta=\frac{5\pi}{6}} = \kappa_0 \begin{pmatrix} \frac{1}{4} e^{i\frac{2\pi}{\Lambda_s}z} - \frac{3}{4} e^{i\frac{2\pi}{\Lambda_l}z} \\ \frac{\sqrt{3}}{4} e^{i\frac{2\pi}{\Lambda_s}z} + \frac{\sqrt{3}}{4} e^{i\frac{2\pi}{\Lambda_l}z} \end{pmatrix} \quad (7)$$

Contrary to the Eq. (6), the coupling strengths in the upper and the lower parts have the sine and cosine functions, respectively as shown in Eq. (7), thereby exhibiting the notch splitting in the odd mode couplings. For the even LP_{11} mode couplings, the maximum notch moves from 1309.1 (θ = 2π/3) to 1307.7 nm (θ = 5π/6) as the angle θ increases. It is because the fraction of the coupling strength having phase term of Λ_l becomes larger. Therefore, the main peak moves from the resonant wavelength satisfying the phase matching conditions of $2\pi/L_B^{LP01\text{-}LP11even} = 2\pi/\Lambda_s$ to that of $2\pi/L_B^{LP01\text{-}LP11even} = 2\pi/\Lambda_l$, which are 1309.8 and 1307.4 nm, respectively.

5. Conclusion and discussion

We successfully identified the origin of the multiple resonance peaks observed in AO coupling in PCFs. We show that the origin is from the ellipticity in fiber outer cladding and the irregularity in the air-hole lattice on the fiber cross-section that results in the acoustic and optical birefringence, respectively, and the angular misalignment between the two birefringent axes. All experimental results are in good agreement with numerical calculation and simulation.

Although the experimental results presented in this paper are for 1200 ~ 1300 nm wavelength range, we actually carried out the same experiments for other wavelengths (600 nm and 900 nm range) and obtained similar results. It should also be mentioned that the formalism developed in this paper can be generalized for any fiber having angular misalignment between the acoustic birefringence axes and the eigen axes of the higher order optical modes involved in the acousto-optic coupling. However, for PCFs with different air-hole configurations, modifications may be required because their mode classification and degeneracy would be different from those of the PCF used in this work [16]. Finally, this study provides means to accurately characterize the optical and the acoustical properties of PCFs, and to improve the performance of AO devices.

Acknowledgment

This work was partially supported by a grant (R08-2004-000-10503-0) from Korea Research Foundation.

#92144 - $15.00 USD Received 28 Jan 2008; revised 3 Apr 2008; accepted 6 Apr 2008; published 16 Apr 2008